

## *Electronic Supplementary Information*

### **Single-Molecule Determination of Chemical Equilibrium of DNA Intercalation by Electrical Conductance**

Lu Zhang, Satoshi Kaneko, Shintaro Fujii, Manabu Kiguchi, and Tomoaki Nishino

#### Contents.

DNA melting studies	2
STM break-junction studies	3
Additional conductance histograms of $I-t$ measurements	4
Conductance values observed in conductance histograms	5
Dependence of peak area of conductance histogram on EB concentration	6
Description of the peak area of conductance histogram by ligand concentrations	7
Spectroscopic determination of the association constants of EB and DNA	9
Experimental procedures	10
References	12

### *DNA melting studies*

We conducted UV-visible spectroscopic studies, as shown in Figure S1, to assess the melting temperature ( $T_m$ ) of the double-stranded DNA (dsDNA) used in the present work. The  $T_m$  value was found to be 36.7 °C, which was more than the room temperature at which the single-molecule conductance and fluorescence spectra were measured. The results prove that dsDNA predominantly exists in the solution and on the substrate. A small fraction of dissociated single-stranded DNA (ssDNA) could be present as a minor species even at room temperature in these experiments. The presence of ssDNA could result in an overestimation of the association constant,  $K_a$ . The degree of the overestimation in  $K_a$  estimated from the single-molecule measurements would be similar to that obtained using ensemble fluorescence titration.

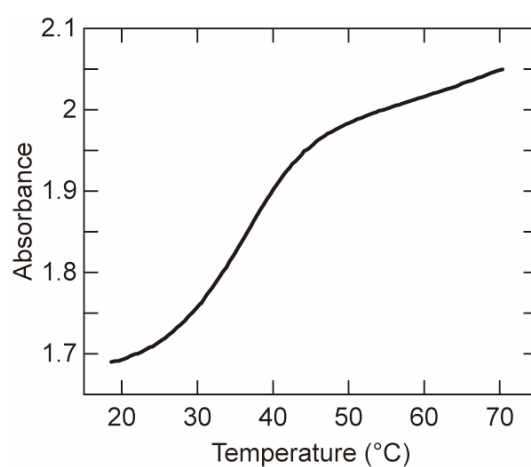


**Fig. S1** Melting curve measured at 260 nm. The sample solution was prepared by dissolving DNA at a concentration of 5.0  $\mu$ M in 0.1 M phosphate-buffered saline (PBS; pH 8.0).

### *STM break-junction studies*

STM-BJ studies were performed with the substrate immersed in a PBS solution containing 1.0  $\mu\text{g/ml}$  EB. Plateaus were observed in the resulting traces, and a clear peak appeared in the conductance histogram (Fig. 1c). The single-molecule conductance of EB was consequently determined to be  $6.1 \times 10^{-4} G_0$ , which is in accordance with our earlier report.<sup>1</sup> The substrates modified with a PBS solution containing both 1.0  $\mu\text{M}$  DNA and 1.0  $\mu\text{g/ml}$  EB were also analyzed using the STM-BJ method to characterize the product of the complexation reaction between DNA and EB. The plateaus observed in the traces caused the appearance of a single peak in the conductance histogram, as shown in Fig. 1d. The peak was located at  $2.2 \times 10^{-3} G_0$ , which corresponds to none of the DNA or EB single-molecule junctions. We ascribed the observed junction in Fig. 1d to the single-molecule junction of the DNA–EB complex, and this conclusion was corroborated by the concentration-dependence studies, as discussed later. A comparison of the histograms in Fig. 1b–d revealed that the single-molecule conductance of DNA increased by an order of magnitude after treatment with EB. The enhanced electron-transport property is explained by the electronic interaction between the bases in DNA and the intercalating EB. It is known that the  $\pi$ – $\pi$  orbital overlaps of the stacked bases mediate electron transport through DNA.<sup>2</sup> The EB intercalation leads to notable electronic interactions with the neighboring DNA bases,<sup>3</sup> and, consequently, the single-molecule conductance of DNA increases upon intercalation, as evidenced by the decrease in the energy of the conducting molecular orbital.<sup>1</sup> In this study, the sample surface was prepared by modification of the substrate in the mixed solution of DNA and EB, but no peak corresponding to the uncomplexed pure DNA or EB appeared in the conductance histogram in Fig. 1d. The absence was most probably due to the large background counts in the histogram, which obscured peaks in the low-conductance region.

*Additional conductance histograms of  $I$ - $t$  measurements.*

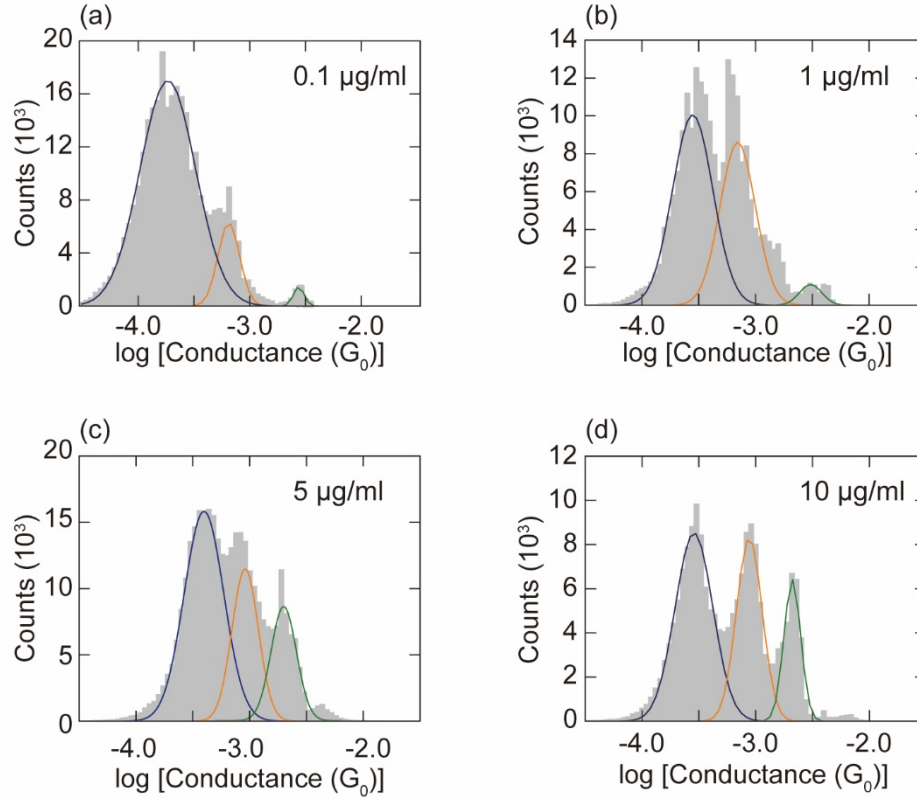


**Fig. S2** Conductance histogram obtained by  $I$ - $t$  measurements. The solution of 1.0  $\mu\text{M}$  DNA and (a) 0.1, (b) 1, (c) 5, and 10  $\mu\text{g/ml}$  EB was used for substrate modification. Bias voltage of 50 mV and set-point current of 5 nA were employed in the  $I$ - $t$  measurements. All the histograms were compiled from 6000 traces. The histograms in b and d are the same as those shown in Figure 2b and c, respectively, but were reproduced for completeness.

*Conductance values observed in conductance histograms.*

**Table S1** Conductance values were determined by the histograms compiled from the  $I-t$  traces. The DNA concentration was kept constant at 1.0  $\mu\text{M}$ .

EB concentration	Conductance / $G_0^a$
0.10 $\mu\text{g/ml}$	$2.0 \times 10^{-4}$ (L), $5.6 \times 10^{-4}$ (M), $2.0 \times 10^{-3}$ (H)
1.0 $\mu\text{g/ml}$	$2.5 \times 10^{-4}$ (L), $7.6 \times 10^{-4}$ (M), $2.8 \times 10^{-3}$ (H)
5.0 $\mu\text{g/ml}$	$3.2 \times 10^{-4}$ (L), $8.3 \times 10^{-4}$ (M), $2.0 \times 10^{-3}$ (H)
10 $\mu\text{g/ml}$	$2.5 \times 10^{-4}$ (L), $7.9 \times 10^{-4}$ (M), $2.1 \times 10^{-3}$ (H)

<sup>a</sup> L, M, and H represent low-, medium-, and high-conductance states, respectively.

*Dependence of peak area of conductance histogram on EB concentration*

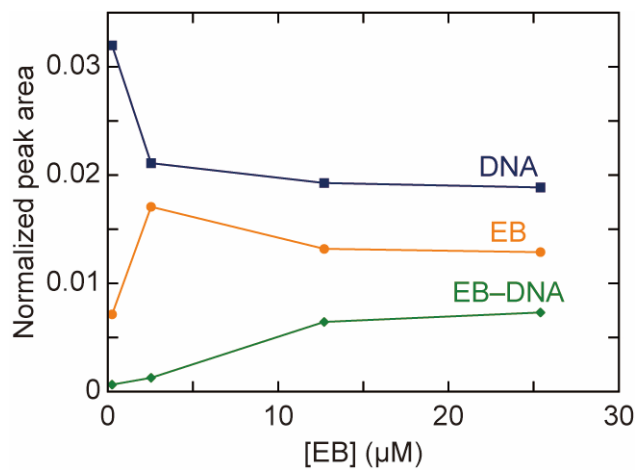


**Fig. S3** Dependence of peak area of conductance histogram on EB concentration. The conductance histograms shown in Figure S2 were used to calculate the peak areas. The peaks for single-molecule junctions of DNA, EB, and EB-DNA were shown in blue (square), orange (circle), and green (diamond), respectively.

### *Description of the peak area of conductance histogram by ligand concentrations*

We recorded current–time ( $I$ – $t$ ) measurements, and the formation of the single-molecule junction, composed of DNA, EB, or the EB–DNA complex, was observed as plateaus in the current traces, as described in the main text. The peak area of the resulting conductance histogram,  $S$ , reflects the sum of the data points in the plateaus of the current traces. Given that the observation probability of the molecular junction,  $P$ , depends on the number of constituent molecules on the surface of the substrate,  $S$  is proportional to the concentration of the molecules in the solution used to prepare the sample surface. Hence, by focusing on the junction of the EB–DNA complex, we obtain:

$$S = \tau P[\text{EB–DNA}], \quad (1)$$

where  $\tau$  is the average lifetime of the molecular junction. Meanwhile, the association constant of EB and DNA,  $K_a$ , is defined as:

$$K_a = \frac{[\text{EB–DNA}]}{[\text{EB}][\text{DNA}]} \quad (2)$$

, where  $[\text{EB}]$  and  $[\text{DNA}]$  denote the concentrations of uncomplexed free EB and DNA, respectively.

By introducing the total concentrations of EB and DNA as  $[\text{EB}]_{\text{tot}}$  and  $[\text{DNA}]_{\text{tot}}$ , respectively, the concentration of the EB–DNA complex can be calculated as:

$$\begin{aligned} & [\text{EB–DNA}] \\ &= \frac{1}{2} \left\{ \frac{1}{K_a} + [\text{EB}]_{\text{tot}} + [\text{DNA}]_{\text{tot}} \right. \\ & \quad \left. - \sqrt{\left( \frac{1}{K_a} + [\text{EB}]_{\text{tot}} + [\text{DNA}]_{\text{tot}} \right)^2 - 4[\text{EB}]_{\text{tot}}[\text{DNA}]_{\text{tot}}} \right\} \end{aligned} \quad (3)$$

Therefore, the peak area of conductance histogram is related to the concentrations; by substituting equation (3) into equation (1), we obtain

$$S = \frac{\tau P}{2} \left\{ \frac{1}{K_a} + [\text{EB}]_{\text{tot}} + [\text{DNA}]_{\text{tot}} - \sqrt{\left( \frac{1}{K_a} + [\text{EB}]_{\text{tot}} + [\text{DNA}]_{\text{tot}} \right)^2 - [\text{EB}]_{\text{tot}}[\text{DNA}]_{\text{tot}}} \right\} \quad (4)$$

Equation (4) is used to determine the association constant from the single-molecule conductance measurements (see the main text). As is well known, the association constant depends on the temperature. This can be addressed by variable-temperature conductance measurements, which have been developed for the study of the thermoelectric effect of single-molecule junctions.<sup>4</sup>

We discuss the robustness of the present method. The conductance of a single-molecule junction in general decreases exponentially under the tunneling mechanism as the molecular length increases. Alternatively, the conductance is inversely proportional to the molecular length when the hopping mechanism predominantly operates in the electron transport, such as the case for DNAs with abundant GC base pairs.<sup>5,6</sup> Thus, the conductance of DNA varies depending on its sequence and length. For the present EB intercalation, we found in the previous study that there exists a distinct difference in the single-molecule conductance between EB–DNA complex and uncomplexed DNA.<sup>1</sup> But this is not the case for uncomplexed EB and uncomplexed DNA: it is possible that the conductance of DNA with a particular sequence and length coincides with that of EB, and, consequently, DNA cannot be discriminated from EB based on the conductance values. Even under this circumstance, we can determine the association constant because, from the conductance histograms, only the peak area of molecular junction of EB–DNA complex is necessary to plot the binding curve (see equation (4) above).



### *Spectroscopic determination of the association constants of EB and DNA*

Fluorescence emission measurements were recorded to determine the association constants of EB and DNA. A solution of EB (1  $\mu\text{M}$ ) was titrated against the DNA solution, which resulted in an increase in the EB fluorescence intensity. Fluorescence intensities normalized with the saturated emission value were plotted against the total DNA concentration. The binding curve was fitted with the following equation under the assumption that each EB molecule was bound to  $n$  molecules of DNA:<sup>1</sup>

$$[\text{DNA}]_{\text{tot}} = n \frac{\Delta F}{F_{\text{max}}} [\text{ligand}]_0 + \left\{ \frac{1}{K_a} \left( \frac{\Delta F / F_{\text{max}}}{1 - \Delta F / F_{\text{max}}} \right) \right\}^{1/n},$$

where  $[\text{DNA}]_{\text{tot}}$  and  $[\text{ligand}]_0$  are the total concentrations of the DNA and ligand (EB), respectively,  $\Delta F / F_{\text{max}}$  is the relative fluorescence increase normalized with respect to the saturated fluorescence intensity, and  $K_a$  is the association constant.

## *Experimental procedures*

**General.** The reagents were of the highest grade available. Deionized water purified with a Milli-Q water purification system (Japan Millipore, Tokyo, Japan) was used for all experiments.

Fluorescence measurements were recorded using an FP-6300 spectrofluorometer at room temperature by titrating a 1  $\mu$ M EB solution against 500  $\mu$ M DNA solution. Fluorescence emission spectra were recorded at wavelengths ranging from 540 to 750 nm upon excitation at 525 nm with a bandwidth of 5 nm for excitation and emission.

**Sample preparation.** The Au(111) substrate was prepared by thermal evaporation on mica under high vacuum.<sup>7</sup> DNA with a sequence of 5'-GCTTGTTG-3' and a  $-(CH_2)SH$  group at the 3' terminal, and its complementary strand were purchased from Tsukuba Oligo Service (Ibaraki, Japan). Each DNA was dissolved at the 100  $\mu$ M concentration in 10 mM PBS. Double-stranded DNA (dsDNA) was prepared by heating the DNA solution at 75 °C for 1 h and then allowing it to slowly cool to room temperature. The mixed solution of EB and dsDNA was prepared by adding 100  $\mu$ g/mL of EB solution to 1  $\mu$ M dsDNA solution. The clean Au(111) substrate was immersed into either the dsDNA solution or the mixed solution of EB and dsDNA for 1 h at room temperature. After immersion, the substrate was carefully washed with pure PBS to remove the physisorbed molecules.

**STM measurements.** Single-molecule conductance measurements were performed on a Nanocute scanning probe microscope system. A Au wire (99.999%, 0.25 mm diameter) was electrochemically etched with 3.0 M NaCl solution in 1% perchloric acid to prepare the STM tips.<sup>8</sup> In STM-BJ measurements, the STM tip was brought into and out of contact with the sample surface at 20 nm/s. Current flowing during tip withdrawal was recorded at a sampling frequency of 20 kHz. For  $I-t$  measurements, the STM tip was held still over the substrate at a fixed tunneling gap with feedback loop disabled, and the current was recorded as a function of time at a sampling frequency of 20 kHz.

Both STM-BJ and  $I-t$  measurements were performed at a bias voltage of 50 mV.

**Data analysis.** STM measurements were repeated using independently prepared tips and sample surfaces to ensure reproducibility. The traces obtained with the STM-BJ measurements were selected by an automated algorithm based on literature.<sup>9</sup> To construct a conductance histogram, thousands of traces were statistically analyzed. Specifically, the conductance value of each data point in the traces as shown in Fig. 1b–d was collected for generating the histogram. Since the plateaus, originated from the molecular junctions, contained numerous data points at similar conductance values, the histogram showed the peak at the conductance. In the case of the  $I-t$  measurements, the junction formation was reflected as the current jumps in the measured traces, as shown in Fig. 2a. These signals were extracted through adaptive threshold analysis developed in our previous study.<sup>10</sup> The current increases from the background set-point current value were calculated for each data point in the  $I-t$  traces, and histograms were constructed after converting the current into conductance. The statistical histogram analyses in the STM-BJ and  $I-t$  measurements reduce the possible effects of current fluctuations inevitable in a single-molecule experiment.

## References

1. T. Harashima, C. Kojima, S. Fujii, M. Kiguchi and T. Nishino, *Chem. Commun.*, 2017, **53**, 10378-10381.
2. S. O. Kelley and J. K. Barton, *Science*, 1999, **283**, 375.
3. S. E. Patterson, J. M. Coxon and L. Strekowski, *Biorg. Med. Chem.*, 1997, **5**, 277-281.
4. Y. Komoto, Y. Isshiki, S. Fujii, T. Nishino and M. Kiguchi, *Chemistry – An Asian Journal*, 2017, **12**, 440-445.
5. B. Xu, P. Zhang, X. Li and N. Tao, *Nano Lett.*, 2004, **4**, 1105-1108.
6. L. Xiang, J. L. Palma, C. Bruot, V. Mujica, M. A. Ratner and N. Tao, *Nat. Chem.*, 2015, **7**, 221-226.
7. P. Wagner, M. Hegner, H.-J. Guentherodt and G. Semenza, *Langmuir*, 1995, **11**, 3867-3875.
8. D. Gingery and P. Bühlmann, *Rev. Sci. Instrum.*, 2007, **78**, 113703.
9. M. S. Inkpen, M. Lemmer, N. Fitzpatrick, D. C. Milan, R. J. Nichols, N. J. Long and T. Albrecht, *J. Am. Chem. Soc.*, 2015, **137**, 9971-9981.
10. T. Harashima, Y. Hasegawa, S. Kaneko, M. Kiguchi, T. Ono and T. Nishino, *Angew. Chem. Int. Ed.*, 2019, **58**, 9109-9113.